Int J Adv Manuf Technol (2013) 68:1517–1527
DOI 10.1007/s00170-013-4939-4

ORIGINAL ARTICLE

A method for thermal performance modeling and simulation of machine tools

Jianfu Zhang · Pingfa Feng · Chuang Chen · Dingwen Yu · Zhijun Wu

Received: 25 June 2012 / Accepted: 21 March 2013 / Published online: 11 April 2013

Abstract The development of precision machine tools requires an accurate understanding of the thermal behaviour of the tools. Therefore, by developing highly accurate machine tool thermal behaviour simulations, it can accurately forecast the functional performance of a machine tool at the prototype design stage and provide guidance on its design and performance optimization. To improve the accuracy of the thermal simulation of machine tools, it proposed whole-machine temperature field and thermal deformation modeling and a simulation method for vertical machining centers. Based on the studies of thermal–structure coupling finite-element data flow and its critical conditions, it also proposed design and computational methods for obtaining the heat-source power, when various rotational speeds, the forced convection heat transfer coefficient between a rotating surface and the air, the combined heat transfer coefficient between a stationary surface and the air/environment, and key contact surface thermal resistances were considered. Furthermore, this paper performed finite-element simulation analysis based on the constructed whole-machine thermal model, and the temperature characteristics and heat deformation mechanism/state were obtained. After comparing the simulation and experimental results, it verified the effectiveness of the finite-element simulation model and the relevant methods and confirmed that the simulation accuracy for both the temperature characteristics and the thermal deformation had been improved significantly, with a simulation error less than 10 %.

J. Zhang (✉) · P. Feng · C. Chen · D. Yu · Z. Wu
The State Key Laboratory of Tribology, Department of Mechanical Engineering, Tsinghua University, Beijing 100084, People's Republic of China
e-mail: zhjfmail@gmail.com

Keywords Machine tool · Thermal simulation model · Temperature field · Thermal deformation

1 Introduction

The errors caused by thermal deformation directly affect the precision of a machine tool. How to improve machine tool thermal performance by reducing thermal deformation and therefore increase its machining accuracy is one of the most important research topics in machine tool design and performance optimization analysis. The relevant research can be summarized into three main categories. The first category is thermal performance testing. Lee [1], Yang [2], Ramesh [3, 4], and Chen et al. [5] proposed test methods for thermal performance, thermal error detection and modeling, and temperature and thermal deformation characteristics in a relatively accurate fashion, based on the constructed test environment. The second category is thermal performance optimization and compensation. Ramesh [6] systematically reviewed the research on thermal performance compensation over the past ten years. Wu [7] and Lee et al. [8] performed precision modeling and error compensation research based on thermal performance analysis, then proposed real-time compensation methods, and modeled thermal errors to optimize the thermal performance of machine tools. Yang et al. [9, 10] proposed a novel modeling methodology for machine tool thermal error compensation by combining the advantages of both gray model and artificial neural network in terms of data processing. The third category is the simulation of thermal performance. For example, aiming to predict and control thermal behaviour, Zah [11] described a numerical method for determining thermally induced errors. Gomez-Acedo [12] proposed a method specially designed for the assessment of repeatability and accuracy of large

machine tools along with results for a large gantry-type milling machine. Zhao [13], Cui [14], and Creighton [15] discussed methods of setting the thermal load and boundary conditions of a motorized spindle, where the thermal characteristic simulation analysis of a motorized spindle was achieved, and the temperature field and thermal errors of the spindle were dynamically simulated.

In general, the quality of a machine tool depends on its design and manufacture. Therefore, the highest priority is to accurately predict and grasp various aspects of the performance and machining accuracy. However, due to some reasons, the analysis results are often significantly different from the actual performance and cannot be used as a reliable basis for design. As a result, the traditional process of "design-develop-test-modify" is usually adopted, whereby the experimental prototype is designed and developed; the performance parameters are obtained by carrying out relevant performance tests on the prototype; and then, either performance optimization or thermal error compensation, depending on the test results, is used to eliminate design flaws. This process usually results in a long production cycle and a high cost, mainly due to the complexity of the machine tool structure and the thermal deformation process, as well as the lack of perfect norms and methods.

There are several major challenges for state-of-the-art machine tool thermal performance simulation. Most studies focused on the thermal deformation simulation of spindle system parts and lacked a highly reliable whole-machine digital simulation model. Consequently, such studies can reflect the thermal deformation process of the spindle system to a certain extent but cannot produce a true reflection of the actual situation of the whole-machine thermal deformation. In contrast, the accuracy of machine tool thermal performance mainly depends on the definition of various initial conditions and the appropriate simulation of boundary conditions, so it is essential to develop a more comprehensive and accurate thermal performance simulation and analysis modeling method to guide its design and performance optimization. The existing machine tool thermal performance simulation models mainly considered the internal thermal sources and thermal dissipation boundary conditions but rarely considered the influences from thermal contact resistance among the machine tool joints or from differing spindle thermal performance under various rotational speeds. All of the above drawbacks resulted in poor simulation accuracy and incorrect predictions of thermal deformation in the whole machine.

This paper firstly proposed and constructed a whole-machine temperature field and thermal deformation simulation method for a vertical machining center. Furthermore, a method was systematically presented for definition of the initial and boundary conditions for the thermal performance simulation of machine tools. It then discussed key issues, including thermal simulation boundary condition, such as thermal sources, heat transfer coefficients, and contact resistance, and associated computational methods. Finally, it discussed the mechanism of deformation and the characteristics of whole-machine temperature fields and thermal deformation under various spindle rotational speeds and verified the accuracy of the proposed methods and finite-element models by comparing the simulation results with the experimental results.

2 Analysis of machine tool thermal performance simulation method

2.1 The thermal performance simulation model

This study was primarily conducted by using a type of mass-produced vertical machining center. As shown in Fig. 1a, the main parameters of the machine tool are listed as follows: (1) *X*/*Y*/*Z*-axis travel, 1,100/510/575 (millimeter); (2) *X*/*Y*/*Z*-axis rapid traverse, 36/36/30 (meter per minute); (3) maximum spindle speed, 8,000 rpm; and (4) spindle motor power, 7.5/11 kW. The spindle system has no cooling circulation.

To fully consider the heat transfer correlation and structural constraints among various parts in the vertical machining center, the whole-machine modeling method was adopted. For whole-machine finite-element simulation modeling, the coordinates of the saddle, the table and the headstock were chosen to represent those used for the thermal performance experiments. At the same time, a simulation model consisting of the bed, saddle, table, column, headstock, spindle assembly, and BT40 standard test bar was constructed.

Because of the complexities of the shapes of the vertical machining center, some unimportant characteristics including holes, small stairs, chamfers, and bolt holes were simplified during the generating of the whole-machine 3D finite-element model before meshing by validating their influences on the simulation accuracy through simulation experiment. It avoided too many grids and units that would otherwise affect the computational time for finite-element simulation [16, 17]. This study meshed the grids by treating the vertical machining center as a whole. Because most of the parts of the vertical machining center have irregular geometric shapes, this paper adopted an automatic partitioning method for meshing, if a part with a regular geometrical shape would generate a hexahedral mesh and a part with an irregular geometrical shape would generate a tetrahedral mesh. There were 191,057 units and 487,734 nodes in the whole-machine finite-element simulation model after the automatic partitioning, as shown in Fig. 1b.

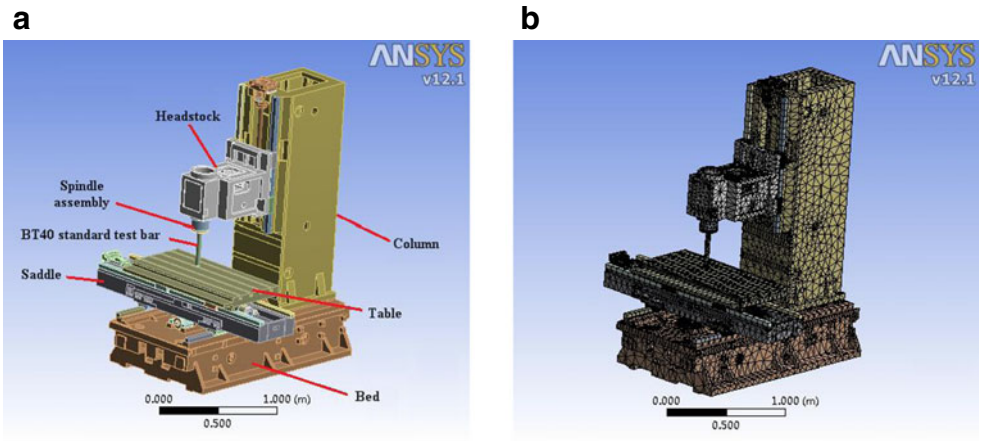

Fig. 1 FEM model of the vertical machining center

Numerical Model Mesh model

2.2 The thermal–structure coupling finite-element simulation method

The heat passage in various components of the machine can be divided into three types: heat conduction, convection, and thermal radiation. Heat conduction, also referred to as the thermal conductivity, is the main heat transfer form. For example, inside the vertical machining center, heat passes from the bearings to other parts in the form of heat conduction. Thermal convection relies mainly on the transfer of heat, such as air, oil, and fluid movement. For example, heat is transferred between the vertical machining center and the ambient air, lubricating oil, and coolant in the form of convective heat transfer. Thermal radiation transfers heat through the surfaces by emitting electromagnetic waves that transmit heat to the environment. The vertical machining center exchanges heat with the surrounding environment at all times by transmitting and receiving electromagnetic waves, a form of radiation heat transfer.

The numerical calculation methods for the temperature field and thermal deformation in a vertical machining center include the finite difference method, the boundary element method, and the finite-element method. This paper adopted the finite-element method to analyze the distribution of the temperature field and thermal deformation of the vertical machining center. Typically, thermal coupling analysis methods can be classified into the direct coupling method and the sequential coupling method. The direct coupling method is only an analysis process, and the unit used includes all degrees of freedom. This method applies a direct calculation to cover all of the necessary physical load vectors, the unit matrix, and the load vector matrix to achieve the coupling. The sequential coupling method contains two or more different physical analysis methods by priority. The results of the former analysis served as the load to the latter analysis to achieve the coupling. Thermal–structure coupling is a typical sequential coupling method that requires three steps: (1) the establishment of the thermal performance unit analysis model, the definition of the conditions for the thermal performance analysis, and the acquisition of the temperature field of the whole-machine tool by thermal analysis; (2) the conversion of the model units into the corresponding structural units, the addition of the temperature field obtained through the thermal analysis to the structural analysis as the load; and (3) the definition of the boundary conditions for the structural analysis, and the computation of the thermal deformation of the machine tool by structural analysis. The data flow of the thermal–structural coupling finite-element analysis used in this study is shown in Fig. 2.

3 Definition of the initial and boundary conditions

The most important part of machine tool thermal performance analysis is the determination of the initial conditions and boundary conditions of the finite-element simulation based on the characteristics of the machine structure and the thermal properties. These conditions include the followings: (1) analysis of thermal sources, such as the spindle electrical heating power and spindle bearing heating power; (2) analysis of heat transfer coefficients, such as the forced convection heat transfer coefficients between the rotating surfaces of the spindle, the taper shank, the test stick, and the air, and the composite heat transfer coefficients between the static surfaces of the bed, saddle, workbench, column and the headstock and the air/environment; (3) analysis of thermal contact resistance, such as the thermal contact resistance between the spindle -inner ring and the spindle, the spindle bearing outer ring and the sleeve, the spindle sleeve and the headstock, the spindle taper sleeve and the test rod, and the slider and the column guide; and (4) thermal state analysis of the initial conditions, such as the initial

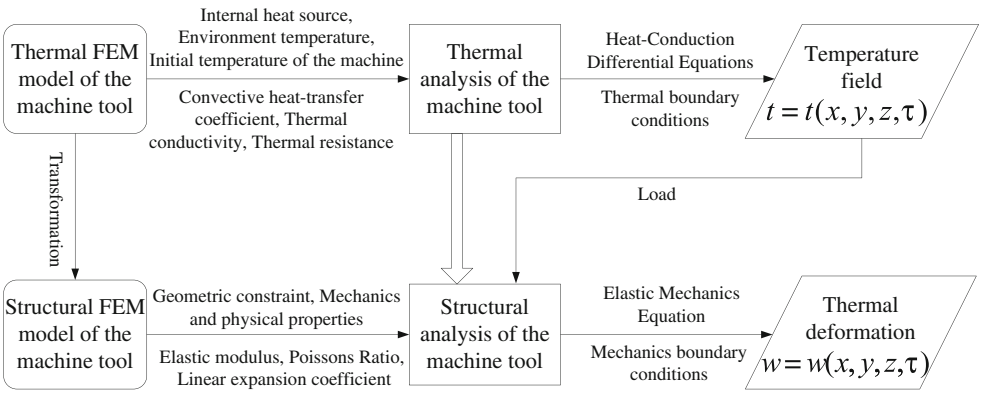

Fig. 2 Thermal–structural coupling finite-element analysis process

temperature, the ambient temperature, and the thermal parameters for the various materials of which the various parts of the machine tool are made. This paper elaborates these key issues from four aspects.

3.1 Thermal source analysis

Machine tool thermal sources are usually divided into two types: internal and external heat/thermal sources. Internal thermal sources include power loss of the spindle motor, spindle bearing friction heat, friction heat of the headstock pulley transmission, three-axis drive motor power loss, slider rail friction heat, friction heat of the lead screw nut, electrical components, tool-drive motor heating, cutting-induced heat, and other similar effects. Among these sources, the power loss of the spindle motor and the spindle bearing friction heat are the most important internal heat sources. As long as the spindle is in the rotational running state, these two sources of heat always exist, and internal heat dissipation will lead to heat deformation and relative displacement of the machine parts; thus, these heat sources have the great impact on temperature elevation and thermal deformation of the spindle components and headstock. Moreover, the cutting heat, generated from cutting the work pieces, transfers to the working piece and the machine tools, leading to deformation caused by temperature elevation; at the same time, the cutting heat can also be transferred from the cutting tools to the spindle taper sleeve, where it then transfers to inside the machine tool, leading to machine tool temperature elevation and heat deformation. The cutting heat is transferred away by the cooling chips and coolant and also has an impact on the temperature of the machine bed, workbench and fixtures, thus causing thermal deformation and degradation of the mechanical machining accuracy. In the process of using a rapid automatic tool changer and cutting feed, the three-axis drive motor power loss, slider rail friction heat and screw nut friction heat also impact the temperature distribution of the machine bed, saddle, workbench, column, and headstock, causing thermal deformation of the whole machine and thus degrading the mechanical machining accuracy. Besides, the external heat sources include the environmental temperature change, air flow, solar radiation, lighting, geothermal effects, heating, and the operator's body temperature. The external thermal sources mainly influence the temperature field and the thermal deformation of the whole machine. Although there is little local change, this impact on machining precision cannot be ignored. The working environment of a high-precision machine tool should be that of a constant-temperature workshop to maximally reduce the machining error caused by whole-machine heat deformation caused by external heat. This paper mainly focused on the thermal performance of the machine tool and the spindle system under various rotational speeds. The cutting heat was not taken into consideration, and the external heat sources were simulated with specific values of the environment temperature and machine tool heat exchange coefficient [18].

Based on the analysis above, the heat power analysis for the spindle motor and bearings among the main heat sources were calculated as shown below. For this study, the spindle system used was a corporate-made mechanical spindle without a cooling system, and the spindle motor model used was the FANUC α8/8000 with a rated power P=7.5 kW, efficiency factor η=77 %, and loss power $P_s=P(1-\eta)/\eta$=2.24 kW. No cooling fan was set on top of the spindle motor for fan cooling. Based on past experience, the power transferred from the motor to the headstock was approximately 30 W. The spindle bearings used were NSK 7014C angular contact ball bearings, the parameters of which are listed in Table 1.

While the spindle bearings were in motion, the bearing inner race-driven rolling element and the bearing cage rotated at high speed, and friction heat was generated by the relative movements between the various parts of the bearing and the lubricant. The bearing friction heat power was related to the friction torque it withstood and can be calculated using formula (1) [19]:

Table 1 Bearing parameters of the spindle system

Bearing type	Contact angle (α)	D (mm)	d (mm)	C_r (N)	C_0 (N)	Speed (rpm)	
						Grease lubrication	Oil lubrication
7014CTYNDBBLP4	15°	110	70	47,000	43,000	12,800	19,500

$$H_f = 1.047 \times 10^{-4} nM \tag{1}$$

where H_f is the bearing friction power in units of watts, n is the spindle speed in units of rpm, and M is the bearing friction torque in units of Newton millimeter.

Based on different friction objects, the bearing friction torque can be composed of two parts and can be calculated using formula (2):

$$M = M_l + M_v \tag{2}$$

The mechanical friction torque M_l depended on the structural parameters of the bearing itself, the load it withstood, and its lubrication method. In this study, the spindle of the vertical machining center was set vertically, and the bearing group used four 7014C bearings installed back-to-back. There was no load toward the radial direction while there was zero load; thus, F_γ=0. The axial load came from the preload force and the spindle gravity after installing the test bar. The designed theoretical preload force for a single bearing was 290 N, and the force of gravity a single bearing withstood was 62 N. Therefore, the axial load withstood by the spindle bearing was 352 N, and the bearing pitch diameter d_m was the average of the bearing inner and outer diameters. The X_0 and Y_0 values of the bearing were set to 0.5 and 0.46, respectively [20].

By combining the data and formulas listed above, the mechanical friction torque for the bearing can be calculated as shown in Table 2.

The viscous friction torque M_v is generated by the relative friction among the rolling elements of the bearing, the cage, and the lubricant. In this study, the viscous friction torque for the angular contact ball bearings was calculated using formula (3) [22]:

$$M_v = \begin{cases} 10^{-7} f_0 (\upsilon n)^{\frac{2}{3}} d_m^3 & \upsilon n \geq 2,000 \\ 160 \times 10^{-7} f_0 d_m^3 & \upsilon n < 2,000 \end{cases} \tag{3}$$

Where υ is the kinematic viscosity of the lubricant under working temperature in units of millimeter squared per second, n is the rotational speed in units of rpm, and f_0 is a coefficient, the value of which is dependent on the bearing parameters and the type of lubricant used.

The vertical machining center was used with German FAG L252 lubricant grease, the kinematic viscosity of which is ≥2 mm^2/s at 40 °C, and the designed rotational speed was 80~8,000 rpm. When the spindle rotational speed is faster than 1,000 rpm and υn≥2,000, formula (3) can be used. If the single-row angular contact bearing lubrication coefficient value f_0 is 2, then the bearing viscous friction torque can be calculated using formula (4):

$$M_v = 10^{-7} \times 2 \times (\upsilon n)^{\frac{2}{3}} \times 90^3 \tag{4}$$

By combining the data and formulas listed above, the friction heat powers of the single bearing for the vertical machining center at various rotational speeds were calculated in Table 3.

3.2 Machine tool heat transfer coefficient analysis

3.2.1 Forced convection heat transfer between rotating body surfaces and the air

The rotating bodies that are exposed to the air while rotating at certain speeds, such as the spindle, taper shank, and test bar, produced relative movement between the surfaces and the nearby air, thus generating forced convection heat transfer. The convection heat transfer coefficient can be calculated using Nusselt's equation [11]:

$$\alpha_f = \frac{N_{u_{\text{air}}} \cdot \lambda_{\text{air}}}{d_s} \tag{5}$$

where a_f is the forced convection heat transfer coefficient between the rotating surfaces and the air, λ_{air} is the thermal conductivity of the air, and d_s is the equivalent

Table 2 Calculation of the mechanical friction torque

Notion	Symbol	Value	Calculation formula
Calculated load of the friction torque (N)	F_β	352	$F_\beta = F_\alpha - 0.1F_\gamma$ [21]
Equivalent static load (N)	P_0	161.92	$P_0 = X_0F_\gamma + Y_0F_\alpha$
Coefficient of the mechanical friction torque	f_l	2.06×10^{-4}	$f_l = 0.0013(P_0/C_0)^{0.33}$
Mechanical friction torque (N mm)	M_l	6.53	$M_l = f_lF_\beta d_m$ [21]

Table 3 Single bearing heat power in different spindle speed

Speed (rpm)	Heat power (W)	Speed (rpm)	Heat power (W)
1,000	3.11	5,000	38.84
2,000	9.06	6,000	52.11
3,000	17.17	7,000	66.85
4,000	27.16	8,000	83.01

diameter of the rotating surface, which can be calculated using formula (6) [18]:

$$d_s = \frac{d_1 l_1 + d_2 l_2 + \cdots d_n l_n}{l}, l = l_1 + l_2 + \cdots l_n \tag{6}$$

The equivalent diameter of the spindle and the taper shank's moving surface $d_{s1} = 0.08m$, and the equivalent of the test bar $d_{s2} = 0.04m$. By checking the relevant tables, at 20 °C, the thermophysical properties of dry air are found as shown below:

$$\lambda_{\text{air}} = 0.0259 W/(\text{m} \times \text{K}),$$
$$\nu_{\text{air}} = 15.06 \times 10^{-6} \text{m}^2/\text{s},$$
$$\text{Pr}_{\text{air}} = 0.703$$

The Reynolds number R_e can be calculated using formula (7):

$$Re = \frac{w d_s^2}{n_{\text{air}}} \tag{7}$$

Because the maximum spindle rotational speed of the vertical machining center is 8,000 rpm, it can derive the maximum Reynolds number under the maximum rotational speed $Re = 3.56 \times 10^5 < 4.3 \times 10^5$ and $0.7 < Pr_{\text{air}} < 670$, and therefore, the Nusselt number can be calculated using formula (8):

$$N_{u_{air}} = 0.133 Re^{2/3} Pr_{air}^{1/3} \tag{8}$$

By combining the data and formulas listed above, the forced convection heat transfer coefficients of the rotation surface at various rotational speeds are calculated as shown in Table 4.

3.2.2 Composite heat transfer coefficient between stationary surfaces and the air/environment

For non-rotational stationary surfaces, such as the machine bed, saddle, workbench, column, headstock, and spindle components, which interact with the air mainly through natural convection, heat transfer occurs when the surfaces are exposed to the air and the ambient air does not create large fluctuations in the airstream. In addition, such surfaces

Table 4 Forced convection heat transfer coefficient of the spindle rotation parts

Spindle speed (rpm)	Forced convection heat transfer coefficient (W/m^2 K)	
	Rotation surface of the spindle and tool shank	Test bar surface
1,000	48.1	38.2
2,000	76.3	60.6
3,000	100.0	79.4
4,000	121.2	96.2
5,000	140.6	111.6
6,000	158.8	126.0
7,000	175.9	139.6
8,000	192.3	152.6

experience radiation heat transfer with the surrounding environment. Based on past experimental results, a composite heat transfer coefficient combining convective heat transfer and radiation heat transfer as a composite heat transfer process was used: $\alpha_s = 9.7\ W/(m^2 \cdot^\circ C)$ [14].

3.3 Machine thermal contact resistance analysis

The types of contact between different parts of the machine tool affect the heat transfer among the joint surfaces. Without considering the joint thermal contact resistance, the contact coefficients for the ideal components assume that there is no temperature difference at the joint. In reality, because of multiple factors, such as the flatness of the component surface, the polish of the surface, the oxidation, the residual fluid, the contact pressure, the surface temperature, and the use of thermal grease, there is joint thermal contact resistance and a temperature difference between the two contact surfaces. Therefore, to obtain reliable computational results from the simulation, influences of the joint thermal contact resistance needed to be considered.

In the thermal state simulation of the Ansys software, the properties for contact surfaces have a “thermal conductance” option, and the value of this option is the reciprocal of the surface thermal contact resistance. By setting the value of this

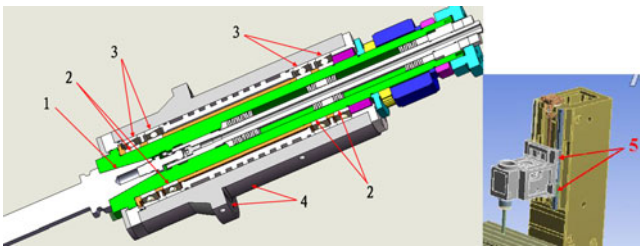

Fig. 3 Identification and setting of thermal contact resistances

Table 5 Thermal contact resistances of key machine tool joints

No.	Joint surface	Thermal resistance (m^2 °C/W)
1	Test bar-holder/spindle taper hole	2.00×10^{-3}
2	Bearing inner ring/spindle	1.37×10^{-4}
3	Bearing outer ring/spindle sleeve	6.06×10^{-4}
4	Spindle sleeve/headstock	1.13×10^{-3}
5	Guideways between headstock and column	1.67×10^{-3}

option, it can add the thermal contact resistance for the joints. This paper considered the thermal contact resistance for the main joints affecting machine thermal transfer and deformation. As shown in Fig. 3, these thermal contact resistances were observed on the following joints: (1) between the spindle and the test bar [23], (2) between the spindle-bearing inner surface and the spindle, (3) between the spindle-bearing outer surface and the spindle sleeve, (4) between the spindle sleeve and the headstock, and (5) between the slider and the column guide.

By defining the material properties, surface morphology, contact medium, and pressures on both sides of the joints into the thermal contact resistance database (co-developed by the project team), the thermal contact resistances for the key machine tool joints can be obtained, as shown in Table 5.

3.4 Definitions of the thermophysical parameters for the machine tool materials

For the finite-element simulation of the temperature field and the thermal deformation of the vertical machining center, the thermal sources and the heat transfer boundary conditions needed to be determined. It is also necessary to define the thermophysical parameters of various machine tool materials. The main material used for machine tool parts is 20Cr, 45# steel, and the material used for machine components (such as the headstock and column) is HT300. Using the natural convection of air in the external environment, thermo-physical parameters of the machine tool materials are listed in Table 6.

4 Discussion of thermal performance simulation and experimental results

4.1 Temperature field and thermal deformation analysis

To study the thermal performance of the vertical machining center, this paper performed temperature field and thermal deformation simulation analysis for a machine tool spindle with 6000-rpm rotation as an example. As a reference to the initial temperature value at the spindle flange for this experiment, the initial temperature for the whole machine was set to 20.1 °C. The thermal boundary values at different spindle rotational speeds obtained from Section 3.3, and the thermal contact resistance at the joints are applied to the whole-machine finite-element model. The whole-machine temperature field obtained from the thermal analysis and simulation is shown in Fig. 4a. Furthermore, the temperature field obtained through the simulation is used as the boundary condition, with fixed and constrained the bottom of the machine bed, and structural analysis of the whole machine is performed. The whole-machine *X*/*Y*/*Z* 3D structural deformation obtained through the simulation under the influence of thermal loads is shown in Fig. 4b–d.

According to the temperature field plot in Fig. 4a, the heat was mainly concentrated on the spindle components and the headstock. Because of the thermal contact resistance at the joints, a small portion of the heat passed into the column through the slider and rails, but the column temperature elevation was relatively small. In the headstock, near the location of the spindle bearing and the motor, the temperature elevation was relatively large. Overall, the temperature distribution was consistent with the experimental results.

Based on 3D thermal deformation plots in Fig. 4b–d, it can make several observations. Firstly, the thermal deformation of the machine tool in the *X* direction was mainly caused by the thermal expansion of the heated headstock and its deformation in the *X* direction. Because the machine bed, column, and spindle components were basically symmetrical, the heat distribution on the machine bed and the column was relatively sparse, and their deformation in the *X* direction had little influence on the whole machine.

Table 6 Thermophysical parameters of the machine tool materials

	Spindle assembly	45# steel	Machine tool parts	Air
Elastic modulus (Mpa)	210,100	209,000	130,000	–
Poisson ratio	0.3	0.269	0.26	–
Linear expansion coefficient (1/K)	1.13×10^{-5}	1.159×10^{-5}	1.1×10^{-5}	–
Thermal conductivity (W/m K)	50.66	49.8	45	2.554×10^{-2}
Specific heat capacity (J/kg K)	477	486	510	1.0069
Density (kg/m^3)	7,830	7824	7300	1.1769

However, the spindle component was installed on the headstock, and it was axisymmetric with the joint surface of the headstock; this component was evenly and symmetrically heated, which had an influence of a relatively small order of magnitude along *X* direction thermal deformation only through the expansion and thermal bending of the thermal test bar. The headstock along the left and right directions was not strictly symmetrical, and the heat it received was also asymmetrical; therefore, this headstock was the most critical factor affecting the *X* direction thermal deformation of the vertical machining center.

Secondly, the *Y* direction thermal deformation of the vertical machining center was also caused by the thermal expansion of the headstock. Because the headstock was not a symmetrical structure in the *Y* direction and the spindle was positioned only on one side of the headstock, the heat generated by the spindle bearing was transferred to the headstock through the spindle sleeve, and the motor-generated heat was also transferred to the headstock. The other end of the headstock was constrained with respect to the column by four sliders and one nut, and the column was also constrained with respect to the machine bed. Eventually, the headstock expanded in the *Y* direction, and the position of the spindle axis also moved in the *Y* direction, which was expressed as whole-machine thermal deformation in the *Y* direction.

Finally, the thermal deformation of the vertical machine center in the *Z* direction was caused by two main factors. The first factor was the thermal expansion in the *Z* direction of the spindle components, mainly resulting from spindle bearing heating, and the second factor was the expansion and bending distortion of the headstock in the *Z* direction, mainly resulting from the superposition of spindle bearing heating and motor heating.

4.2 Comparison of simulation and experimental results

To verify the effectiveness of thermal performance modeling and simulation methods, the same basic conditions were applied for the experiment, and the measurement points

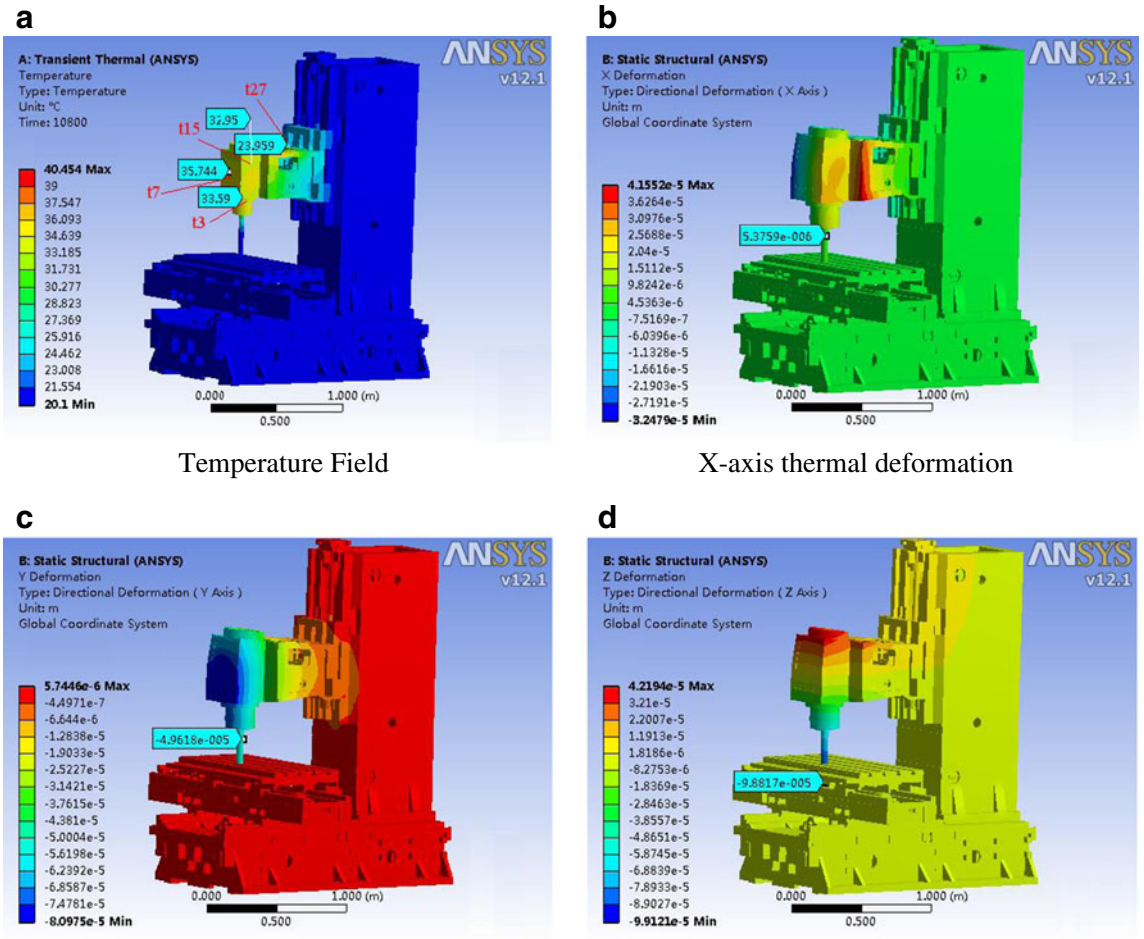

Temperature Field

X-axis thermal deformation

Y-axis thermal deformation

Z-axis thermal deformation

Fig. 4 Simulation results of the thermal performance/6,000 rpm

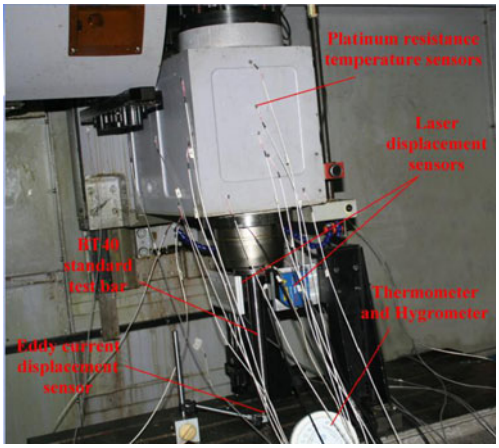

Fig. 5 The thermal performance experimental platform

and deformation test positions were also set to be the same as simulation. The experimental platform is shown in Fig. 5.

The experimental methods, data acquisition, and analysis can be obtained from reference [5]. Thirty two platinum resistance temperature sensors, used to achieve the temperature fields over the whole-machine tool, were mainly arranged onto the surface of the spindle components and headstock. Two laser displacement sensors were fixed on the worktable to measure the thermal deformation of the *X*- and *Y*-axis. The direction of the laser beam and the distance between the laser displacement sensors and the spindle test bar are adjusted, to make sure the laser beam is aligning to the center of the spindle test bar along the axis and focusing on the surface of the spindle test bar. And an eddy current displacement sensor was placed below the bottom of the spindle test bar to detect the *Z*-axis thermal deformation. The displacements between displacement sensors and measured position are adjusted to make sure that it is within their measurement ranges. The temperature field curves and thermal deformation curves from original experimental data are shown in Fig. 6, under 6,000-rpm spindle rotational speed.

It adopted the same methods to perform a finite-element simulation of whole-machine thermal performance for spindle rotational speeds of 4,000 and 8,000 rpm. It then organized the simulation results and compared them with the results obtained from the vertical machining center thermal performance experiments to verify the accuracy of the simulation. Based on the simulation and experimental analysis of the whole-machine temperature field, four corresponding thermal-critical points were selected from both the simulation and experiment for thermal property analysis. Those selected points were the t3 sensor on the spindle flange, the t7 sensor on the spindle bearing on the front surface of the headstock, the t15 sensor on the left central region of the headstock, and the t27 sensor located at the intersection of the upper right corner of the headstock and the slider. The simulated thermal performance of these four sensor points was compared with the experimental measurements, and the results are shown in Table 7.

As it can be drawn form Table 7, the simulated values and the experimental values were found to be in good agreement. The simulation error was less than 10 %. And it shows that the thermal performance simulation model proposed by this study is accurate. Based on the obtained whole-machine temperature field, the thermal deformation simulation was then performed. The results for the whole-machine thermal deformation finite-element simulation are compared with the experimental results in Table 8.

As shown in Table 8, the simulation errors in the *X* direction were relatively high under various rotational speeds but appeared to follow the same rule. This result occurs mainly because the whole-machine thermal deformation value in the *X* direction was relatively small, although an equally significant amount of system absolute error was introduced into the experimental measurement (for example, when the environmental temperature rises one degree, the error introduced due to the *X* direction displacement measurement device deformation would be approximately 2.76 μm). This level of system error has a greater influence on the relative error for the *X* direction thermal deformation measurements than those in the other directions. In contrast, the heat sources in the *X* direction were symmetrically distributed in the whole-machine simulation model. The *X* direction thermal

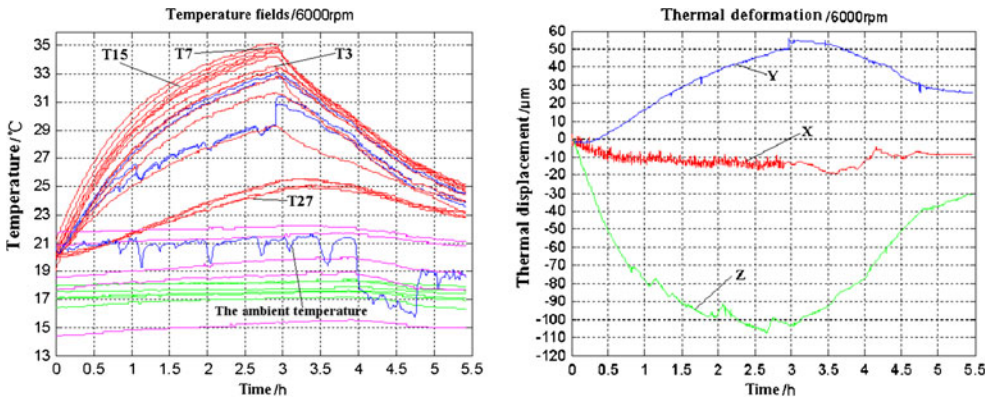

Fig. 6 The experimental temperature fields and thermal deformation

Table 7 Comparison of the simulation and experimental results of the temperature fields

Spindle speed (rpm)	No. of the critical temperature measuring points	Experimental values (°C)		Simulation values (°C)		Simulation error (%)
		Initial temperature	Finish temperature	Initial temperature	Finish temperature	
4,000	t3	16.8	23.5	17.0	24.050	5.22
	t7	17.0	25.0	17.0	25.677	8.46
	t15	17.2	25.3	17.0	24.410	−8.52
	t27	17.2	20.7	17.0	20.210	−8.29
6,000	t3	20.1	33.2	20.1	33.590	2.98
	t7	20.4	34.8	20.1	35.744	8.64
	t15	20.6	34.3	20.1	32.950	−6.20
	t27	20.5	24.7	20.1	23.959	−8.12
8,000	t3	18.1	40.8	18.1	40.124	−2.98
	t7	18.4	42.7	18.1	43.918	6.25
	t15	18.6	41.3	18.1	39.276	−6.71
	t27	18.5	25.8	18.1	24.709	−9.47

deformation value generated purely by the spindle bearing heat and motor heat was, in theory, very small, ignoring the heat and structural complexities introduced by other structures. For the *Y* direction and *Z* direction thermal deformations, the simulation results match with the experimental results under various rotational speeds, and the simulation error was under 10 %. Overall, the simulation results obtained using the thermal performance simulation model developed in this study were consistent with the experimental results. Therefore, this modeling and simulation method can be used to guide digitalized machine tool prototype design and optimization.

5 Conclusion

The thermal simulation accuracy of a machine tool mainly depends on the simulation model and the appropriate definition of various initial conditions and simulation boundary conditions. Therefore, it is critical to have a comprehensive and accurate machine tool thermal performance simulation modeling method to guide its design and optimization. This paper discussed the thermal performance simulation techniques taking a vertical machining center for example, proposed a finite-element modeling method for the whole-machine thermal performance by considering simulation boundary conditions, and studied the data flow and the necessary initial and boundary conditions for the thermal–structural coupled finite-element simulation method. Based on the analysis of machine tool heat sources, heat transfer coefficients, thermal contact resistance, the spindle heating power under various rotational speeds, the forced convection heat transfer coefficient between the air and rotating surfaces, such as the spindle, the taper shank and the test bar, the composite heat transfer coefficient between static surfaces of the machine tool and the air and environment, and the computational methods for five critical thermal contact resistances were calculated and achieved. It also performed finite-element simulation for the whole-machine thermal performance under various rotational speeds and analyzed the distribution of the whole-machine temperature field and mechanism and the forms of thermal deformation. After comparing the simulation results with the experimental results, the simulated whole-machine thermal deformation characteristics exhibited good agreement with the experimental results. The simulation errors of the temperature fields and the thermal deformation along the *Y* and *Z* directions were all less than 10 %, and thus, it verified the effectiveness of the relevant methods and the simulation model proposed by this study.

Table 8 Comparison of the simulation and experimental results of the thermal deformations

Spindle speed (rpm)	Thermal deformation direction	Experimental values (μm)	Simulation values (μm)	Simulation error (%)
4,000	*X*	−7.5	−3.919	−47.8
	Y	41.0	44.321	8.1
	Z	−92.0	−84.518	−8.1
6,000	*X*	−17.6	−5.376	−69.4
	Y	51.6	49.618	−3.8
	Z	−109.0	−98.817	−9.3
8,000	*X*	−18.0	−10.173	−43.5
	Y	110.0	105.710	−3.9
	Z	−210.0	−202.660	−3.5

Acknowledgments This research was financially supported by the Key National Science and Technology Projects of China (grant no.

2012ZX04002-061) and the State Key Laboratory of Tribology Foundation (grant no. SKLT11C7).

References

1. Lee DS, Choi JY, Choi DH (2003) ICA based thermal source extraction and thermal distortion compensation method for a machine tool. Int J Mach Tool Manuf 43(6):589–597
2. Yang SH, Kim KH, Park YK (2004) Measurement of spindle thermal errors in machine tool using hemispherical ball bar test. Int J Mach Tool Manuf 44(2–3):333–340
3. Ramesh R, Mannan MA, Poo AN (2002) Support vector machines model for classification of thermal error in machine tools. Int J Adv Manuf Technol 20(2):114–120
4. Ramesh R, Mannan MA, Poo AN (2003) Thermal error measurement and modelling in machine tools. Part I. Influence of varying operating conditions. Int J Mach Tool Manuf 43(4):391–404
5. Chen C, Zhang JF, Wu ZJ, Feng PF (2011) Real-time measurement of machine tool temperature fields and their effect on machining errors. Mechanika 17(4):413–417
6. Ramesh R, Mannan MA, Poo AN (2000) Error compensation in machine tools—a review Part II: thermal errors. Int J Mach Tool Manuf 40(9):1257–1284
7. Wu H, Zhang HT, Guo QJ, Wang XS, Yang JG (2008) Thermal error optimization modeling and real-time compensation on a CNC turning center. J Mater Process Technol 207(1–3):172–179
8. Lee JH, Yang SH (2002) Statistical optimization and assessment of a thermal error model for CNC machine tools. Int J Mach Tool Manuf 42(1):147–155
9. Zhang Y, Yang JG, Jiang H (2012) Machine tool thermal error modeling and prediction by grey neural network. Int J Adv Manuf Technol 59(9–12):1065–1072
10. Yan JY, Yang JG (2009) Application of synthetic grey correlation theory on thermal point optimization for machine tool thermal error compensation. Int J Adv Manuf Technol 43(11–12):1124–1132
11. Zah MF, Maier T (2010) Thermal simulation of machine tools. Zeitschrift fur Wirtschaftlichen Fabrikbetrieb 105(7–8):655–659
12. Gomez-Acedo E, Olarra A, Lopez de la Calle LN (2012) A method for thermal characterization and modeling of large gantry-type machine tools. Int J Adv Manuf Technol 62(9–12):875–886
13. Zhao HT, Yang JG, Shen JH (2007) Simulation of thermal behavior of a CNC machine tool spindle. Int J Mach Tool Manuf 47(6):1003–1010
14. Cui LY, Zhang DW, Gao WG, Qi XY, Shen Y (2011) Thermal errors simulation and modeling of motorized spindle. Adv Mater Res 154–155:1305–1309
15. Creighton E, Honegger A, Tulsian A, Mukhopadhyay D (2010) Analysis of thermal errors in a high-speed micro-milling spindle. Int J Mach Tool Manuf 50(4):386–393
16. Povilionis A, Bargelis A (2010) Structural optimization in product design process. Mechanika 1:66–70
17. Li HQ, Shin YC (2004) Integrated dynamic thermo-mechanical modeling of high speed spindles, part 1: model development. J Manuf Sci Eng 126(1):148–158
18. Chen C (2011) Study on analysis and optimization for thermal performance of vertical machining center. Tsinghua University, Beijing
19. Chen TY, Wei WJ, Tsai JD (1999) Optimum design of headstocks of precision lathes. Int J Mach Tool Manuf 39(12):1961–1977
20. Okamoto J (2003) Design and calculation of the rolling element bearing. China Machine Press, Beijing
21. Hong RH (2007) Design and thermal characteristic research on high speed permanent magnetic synchronous motorized spindle. Harbin Institute of Technology
22. Dai S (1993) Rolling bearing application handbook of machine tool. China Machine Press, Beijing
23. Xu C, Zhang JF, Wu ZJ, Yu DW, Feng PF (2012) Dynamic modeling and parameters identification of a spindle-holder taper joint. Int J Adv Manuf Technol. doi:10.1007/s00170-012-4586-1